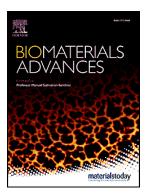
Efficacy of molecular and nano-therapies on brain tumor models in microfluidic devices



Ana M. Martins, Alexandra Brito, Maria Grazia Barbato, Alessia Felici, Rui L. Reis, Ricardo A. Pires, Iva Pashkuleva, Paolo Decuzzi

PII:	S2772-9508(22)00504-0
DOI:	https://doi.org/10.1016/j.bioadv.2022.213227
Reference:	BIOADV 213227

To appear in:

Received date:	10 March 2022
Revised date:	13 October 2022
Accepted date:	28 November 2022

Please cite this article as: A.M. Martins, A. Brito, M.G. Barbato, et al., Efficacy of molecular and nano-therapies on brain tumor models in microfluidic devices, (2022), https://doi.org/10.1016/j.bioadv.2022.213227

This is a PDF file of an article that has undergone enhancements after acceptance, such as the addition of a cover page and metadata, and formatting for readability, but it is not yet the definitive version of record. This version will undergo additional copyediting, typesetting and review before it is published in its final form, but we are providing this version to give early visibility of the article. Please note that, during the production process, errors may be discovered which could affect the content, and all legal disclaimers that apply to the journal pertain.

© 2022 Published by Elsevier B.V.

Efficacy of Molecular and Nano-Therapies on Brain Tumor Models in Microfluidic Devices

Ana M. Martins^{1,*}, Alexandra Brito^{2,3}, Maria Grazia Barbato¹, Alessia Felici¹, Rui L. Reis^{2,3}, Ricardo A. Pires^{2,3}, Iva Pashkuleva^{2,3}, Paolo Decuzzi¹

¹Laboratory of Nanotechnology for Precision Medicine, Istitu'o Italiano di Tecnologia, Via Morego 30, 16163 Genova, Italy

²3B's Research Group, I3Bs - Research Institute on Biomaterials, Biodegradables and Biomimetics, University of Minho, Headquarers or the European Institute of Excellence on Tissue Engineering and Regenerative Medicine, AvePark, Parque de Ciência e Tecnologia, Zona Industrial da Gandra, 4805-017 Barco Cumparães, Portugal;

³ICVS/3B's-PT Government Associate Laboratory, Braga/ Guimarães, Portugal.

*corresponding author: a a.n. artins@iit.it

Highlights

- The importance of microfluidics devices over other 3D organizations, and conventional 2D monolayers;
- Comparative studies on the efficacy of several therapeutic agents such as free DTXL, nanoparticles loaded with DTXL (DTXL-SPN), and Fmoc-Glc6P;
- Fmoc-Glc6P has a selective effect on GBM cancer cells but with no side effects on healthy cells;
- Microfluidic devices are a useful predictive tool to: modeling the *in situ* and systemic administration of chemotherapy in brain tumors

Abstract

The three-dimensional (3D) organizetion of cells affects their mobility, proliferation, and overall response to treatment. Spheroids, organoids, and microfluidic chips are used in cancer research to reproduce *in vitro* the complex and dynamic malignant microenvironment. Herein, single- and double-channel microfluidic devices are used to mimic the spatial organization of brain tumors and investigate the therapeutic efficacy of molecular and nano anti-cancer agents. Human glioblastoma multiforme (U87-MG) cells were cultured into a Matrigel matrix embedded within the microfluidic devices and exposed to different doses of free docetaxel (DTXL), docetaxel-loaded spherical polymeric nanoparticles (DTXL-SPN), and the aromatic N-glucoside *N*-(fluorenylmethoxycarbonyl)-glucosamine-6-phosphate (Fmoc-Glc6P). We observed that in the single-channel microfluidic device, brain tumor cells are more susceptible to DTXL treatment as

compared to conventional cell monolayers (50-fold lower IC₅₀ values). In the double-channel device, the cytotoxicity of free DTXL and DTXL-SPN is comparable, but significantly lowered as compared to the single-channel configuration. Finally, the administration of 500 μ M Fmoc-Glc6P in the double-channel microfluidic device shows a 50% U87-MG cell survival after only 24 hours, and no deleterious effect on human astrocytes over 72 hours. Concluding, the proposed microfluidic chips can be used to reproduce the 3D complex spatial arrangement of solid tumors and to assess the anti-cancer efficacy of therapeutic compounds administrated *in situ* or systemically.

Keywords: microfluidics, glioblastoma, nanomedicine, arti-cancer therapy

1. Introduction

The preclinical screening of new therapies still relies on simplified, two dimensional (2D) *in vitro* models that cannot replicate the biochemical and biophysical complexity of the human diseases [1, 2]. Three-dimensional (3D) cell assemblies, such as cancer spheroids, resemble closer the *in vivo* tissue or generation but cannot reproduce some dynamic processes, *e.g.* mass transport. These processes are crucial for different therapies as they regulate the intra-tissue accumulation of systemically delivered therapeutic agents, the diffusion of nutrients, chemokines and cytokines, as well as the migration and spatial re-arrangement of malignant and healthy cells [3-5]. Microfluidic devices emerged as more accurate tool for screening novel therapies in cancer and other diseases because can replicate both the 3D tissue organization and the thermodynamic/kinetic mechanisms of therapeutics' delivery [6-11]. As examples, microfluidic devices have been designed to model different disorders, including cancer [12-15],

cardiovascular [16, 17], and chronic inflammatory diseases[18]; as well as diverse biological barriers [19-23], such as blood-brain barrier, the intestinal-mucosal barrier, and the alveolar-capillary barrier.

Microfluidic devices for disease modeling can have different configurations with one, two or multiple compartments to mimic the architectural complexity of the native tissue and include tissue/vascular and tissue/tissue biological barriers. Multi-compartment based microfluidic devices comprise two or more channels with different architecta." s to replicate a variety of biological interfaces [10, 24-27]. Different configurations have been efficiently used to model cancer tissues. The group of Huh described a two-comportment device comprising an upper channel that mimic the ductal lumen with pre-assembled cast carcinoma spheroids, and a lower channel, perfused by cell culture media to replicate the breast microvaculature [28]. A thin natural membrane with a layer of stromal cells was interposed between the two compartments. The system was validated by quantifying the anti-proliferative effect of paclitaxel on breast cancer cells. Compartmentalized mic. of uidic systems were also used to study the vascular dynamics of circulating cancer lis, therapeutic responses, and their extravasation/intravasation potential [14, 19, 24, 29-32]. For instance, the metastatic potential of breast cancer cells under different environmental conditions, including the use of inflammatory factors as chemoattractants was quantified with a two-compartment microfluidic device [31]. Habibovic and Reis groups described a "tumor-on-a- chip" model for assessment of gemcitabine-loaded nanoparticles efficacy on colorectal cancer [14]. The viability studies together with live imaging demonstrated a dose dependent effect of gemcitabine loaded nanoparticles to colorectal cancer cells (HCT-116) embedded in Matrigel inside the microfluidic chip [14].

We have been using microfluidic chips with one and two channels [19, 31, 33-37]. The singlecompartment configuration can be used to create simple 'tissue chips', typically, comprises one channel that is filled by a natural hydrogel carrying the cells of interest. In this configuration, the therapeutic agents are administered through one inlet port, directly to the 3D like-tissue, and slowly diffuse towards the opposite outlet port. Such devices have been extensively used to test the vascular transport and adhesion of macrophages [38, 39], cancer cells [31, 37, 40], and nanoparticles [35, 41], under diverse disease conditions. The two compartment configurations usually replicates a single biological interface, either a maschar/tissue or a tissue/tissue interface.[14, 22, 42] In this configuration, one channel a ts as the extravascular compartment (3D like-tissue), which is filled by a natural hydroge¹ carving the cells of interest, while the second channel acts as the vascular compartment (1/10 d vessel), which is continuously perfused by cell culture medium. The therapeutic a yen's are infused through the vascular compartment to simulate systemic administrations or through the extravascular compartment to model direct intra-tissue injections. We have demoi strated the utility of these chips for analysis of vascular and extravascular transport, va. cular transport of circulating tumor cells, immunotherapeutic

Herein, we used these microfluidic devices for *in vitro* testing of model and innovative therapeutic compounds. In the single-channel device, we have a 3D tumor model and simulate the direct injection/application of chemotherapy at the tumor site (i.e. *in situ*). The double-channel microfluidic chip has two parallel channels connected by micropillars - a design that mimics the vascular and parenchymal-cancer compartment to simulate the systemic administration of chemotherapy. Glioblastoma multiforme (GBM) cancer was selected among numerous pathologies because it is referred as the most aggressive and lethal brain tumor in

adults [43]. Previously, we have investigated free docetaxel (DTXL) and spherical polymeric nanocontructs (SPN) loaded with DTXL (DTXL-SPN) for the treatment of cancer cells in conventional (2D) cultures and *in vivo* [44-47]. A biodegradable implant (μ MESH) with docetaxel-loaded nanomedicines directly released into a orthotopic brain cancer model avoided disease recurrence up to eight months after tumor resection [48]. Moreover, since DTXL lacks specificity towards tumor cells, and severe systemic toxicities that triggers huge side effects on patients [49, 50] seems an adequate therapeutic agent to be administrated in a tumor site. Notwithstanding, a new promising selective chemotherapeutic \mathcal{M} (fluorenylmethoxycarbonyl)-glucosamine-6-phosphate (Fmoc-Glc6P), has demonstrated a potent anti-cancer efficacy on osteosarcoma and breast cancer cells [51-53]. In this work, we tested the efficacy of several therapeutic agents such as free DTXL, nanopuliels loaded with DTXL (DTXL-SPN), and Fmoc-Glc6P for comparative purposes [5 -5⁷]. Finally, we hypothesize that Fmoc-Glc6P could be selective also to GBM cancer cells bu, with no side effects on normal cells.

2. Experimental section

All reagents were purchased from Sigma-Aldrich-Merck unless otherwise specified. All experiments were performed in triplicate.

2.1. Fabrication and Characterization of the Microfluidic Chips

In this study, we used two different microfluidic chips: a single- (**Figure 1A**) and double-channel chip (**Figure 1B**), described in detail by Manneschi *et al.* [33] Briefly, a single-channel silicon master template was obtained from a negative template of SU8-50 photoresist. The silicon template was replicated using a mixture of polydimethylsiloxane (PDMS) and sealed with a glass slide. This chip has a length of 27 mm, a height of 42 μ m and a width of 210 μ m (**Figure 1A**).

For the fabrication of the double-channel chips (**Figure 1B**), we used an optical mask of glass together with photolithography to pattern the double-channels into the silicon master chip. The obtained silicon master template was then replicated *via* soft lithography with PDMS. The final PDMS template is composed by two microfluidic channels with a length of 27 mm, interconnected in the middle part by an array of micropillars with 500 μ m in length with a gap size of 3 μ m. The two-channels have a height of 50 μ m and a width of 200 μ m. In these chips the top channel corresponds to the vascular part where the treatment solutions (*e.g.* drugs, nanoparticles, and bioactive compounds) were added; and the botton channel corresponds to the vascular part where the 3D structure of a tumor. This interface between the channels is a permeative micropillar membrane (**Figure 1B**). Each channel has one inlet and one outlet.

Fi jure 1.

2.2. Scanning Electron Microscopy (LFM)

SEM images of microfluidic chips were obtained using the equipment JSM-6490LV, JEOL and Helios Nanolab 650, FEI Contrany. These images were acquired after cutting the chip, bonded on the glass slide, with a blade. The PDMS was sputter-coated with gold. Low-magnification and high-magnification SEM images were obtained with accelerating voltage of 15 and 5 kV, respectively.

2.3. Culture of Human Glioblastoma Multiforme (U87-MG) Cell Lines and Primary Human Astrocytes

The cancer cells were previously transfected with GFP to easily visualize them *in situ* longitudinally with time. U87-MG GFP+ cells were cultured in Minimum Essential Medium Eagle (EMEM) supplemented with 10% heat-inactivated fetal bovine serum (FBS) and 1% penicillin/streptomyocin (P/S). Human cortical astrocytes (#1800, ScienCell Research Laboratories, US) were cultured with astrocytes medium (ScienCell Research Laboratories) with 1% P/S. U87-MG GFP+ and human astrocytes were cultured in T150 flasks until confluence. After the trypsinization, human astrocytes were stained with Vybi.ntTM DiI Cell-Labeling Solution (#V22885, ThermoFisher Scientific), according to the manufacture's protocol. Then, the astrocytes were washed three times with PBS (1X) to remove the excess dye. A concentration of 50:50 Matrigel/cells in EMEM medium were prepared to a final number of 100,000 cells embedded in Matrigel matrix (Corning) per chip. Single- (Figure 1A) or double-channel (Figure 1B) chips were used to culture U87-MG GFP+ cells or astrocytes with Matrigel for 24 hours to form a confluent 3D cell network (Figure 1A – bottom) and then different treatments were applied for 24, 48 and 72 hours. After each time point the cell viability was analyzed by confocal microscopy.

2.4. Treatment Conditions using Single- and Double-Channel Microfluidic Chips Microfluidic chips were terilized in an autoclave at 120 °C. Then, the channels were aspirated within the biohood and the chips were left inside the incubator overnight to dry the remaining water from the channels. U87-MG GFP+ cells or human astrocytes embedded in Matrigel were injected into microfluidic chips and were cultured for 24 hours to form a 3D tumor-like structure. *2.4.1. Single-Channel Microfluidic Chip.* We used the single-channel microfluidics chips to screen several concentrations of DTXL. A stock solution of DTXL (42 mM) was prepared in dimethyl sulfoxide (DMSO). This solution was diluted with EMEM to 0.01, 0.5, 0.1, 1 and 10

 μ M solutions. To assess the cytotoxicity of the anti-cancer drug DTXL, EMEM with different drug concentrations (0.01, 0.5, 0.1, 1 and 10 μ M) was added to the channel inlet and left to diffuse across the 3D tumor-like structure. The therapeutic solution was added every single day to the chip, for up to 72 hours. EMEM was used as a control in this experimental set.

2.4.2. Double-Channel Microfluidic Chip. Three different treatments were investigated: (1) free DTXL (0.01, 0.1, and 10 μ M); (2) spherical nanoconstructs (SPNs) loaded with DTXL (10 μ M) (DTXL-SPN); and (3) 500 μ M free *N*-(fluorenylmethoxycarboxyl)-glucosamine-6-phosphate (Fmoc-Glc6P). All solutions were prepared in EMEM. The UTXL-SPN were fabricated as previously described by us [47]. To assess the drug release kinetics from SPNs, samples were poured in a Slide-A-Lyzer MINI dialysis microtubes with a molecular cut off of 10 kDa (Thermo Scientific) and then dialyzed over PBS buffer at pd 1.4, 37 °C. For each time point, triplicate samples were collected and analyzed $\lambda \nu \nu$ PLC. Fmoc-Glc6P compound was synthesized following the procedure described by three *et al.* [51] The therapeutics were injected into the vascular channels (on the top) every cap. EMEM was used as a control. After 24, 48 and 72 hours, we observed the bottom channel with U87-MG GFP+ cells or human astrocytes embedded in Matrigel, on confident microscope.

2.5. Confocal Microscopy Analysis

Confocal fluorescent microscopy (Nikon A1R+/A1+; objectives Nikon, 10X or 20X) was used to evaluate the cell viability over time. Images were recorded using automated acquisition for Zstack and multicolor channel. Each experiment involved at least five chips per condition and was repeated three times. The same region of interest (ROI) was analyzed at different time points. High-resolution Z-stack images were processed for 3D reconstruction and fluorescence intensity

measurements were performed using NIS-Elements AR (Nikon) software. Cell viability, with EMEM only (control) and after different treatment conditions, was determined measuring the mean fluorescence intensity exhibited by green fluorescent protein (GFP+) cells. Cell viability is presented as percentage, calculated from the fluorescence intensity after 0, 24, 48 and 72 hours. The half-maximal (50%) inhibitory concentration (IC₅₀) was estimated as 50% of cell viability relative to the control (EMEM alone). A logarithmic curve (nonlinear regression) was estimated as the best fitting, and the IC₅₀ for each time point of both experiments was estimated.

2.6. Statistical Analysis

Data are expressed as mean \pm standard deviation. Single (actor analysis of variance (ANOVA) was used to determine statistical significance within a data set. If ANOVA detected a significant difference within the data set, Tukey s lonestly significantly different (HSD) multiple comparison test was used to determine significant differences between groups and conditions.

3. Results and Discussion

Conventional cell culture monolayers poorly recapitulate the native physiology of diseased tissues: they do not reproduce the complex 3D cell organization and the dynamic arrangement under multiple, different physiological clues. On the other hand, microfluidic chips allow to simulate complex cell-culture microenvironments, including the vascular/tissue and tissue/tissue interfaces, spatiotemporal chemical gradients, and mechanical clues of living tissues. Such chips enable the development of new *in vitro* disease models, and might potentially contribute for the replacement, or at least, decrease the number of animal experiments used in drug development and testing [11, 12]. The use of microfluidic devices can overcome several challenges associated

with the animal models, namely cost, labor time, reproducibility, differences with the human physiology, undesired immune responses, and ethical issues. Studies have also suggested that the use of microfluidic devices might accelerate the design of drug-administration regimens for phase I clinical trials [9].

Different therapeutic agents (**Figure 2**), namely free DTXL, DTXL-SPN, and the aromatic Nglucoside Fmoc-Glc6P, were infused in the microfluidic devices and their cytotoxic potential was assessed on cancer cells under different conditions. The potent anti-cancer drug DTXL was considered as a model drug.

In the single-channel configuration, the therapeutic agents were slowly infused through an inlet port and diffused across the whole tumor matrix to react the outlet port. In the double-channel configuration, the therapeutic agents were slowly infused in the vascular channel and perfuse in the extravascular compartments by crossin. The micropillar membrane.

Figure 2.

3.1. Assessing the cytotoxicity of therapeutic agents in the single-channel microfluidic device In the single-channel couffiguration (Figure 1A), 3D tumor-like structure was obtained using U87-MG GFP+ en/bedded in a Matrigel matrix and then the different therapeutics were injected directly throughout the 3D structure. The viability of the tumor cells was estimated by analyzing the variation of the green fluorescent intensity over time: an increase in fluorescent intensity was associated with a higher cell density, thus indicating cell viability; whereas a decrease in fluorescent intensity was associated with a lower cell density, thus indicating cell death. The fluorescent images in Figure 3A-E show variation in cancer cell density within a representative section of the channel (2.9 mm) over time (from 0 to 72 hours) and for different

DTXL concentrations. As expected, the cell viability decreased upon DTXL administration in a time- and concentration-dependent manner. At the lowest concentration of DTXL (0.01 µM), the cell density decreased significantly only after 72 hours (Figure 3A). On the other hand, significantly low cell density was observed after 24 hours at the highest tested concentrations of 1 and 10 µM (Figure 3D, E). Quantitative data for cell viability at the different treatment conditions is presented in Figure 3F and evidence a progressive decrease in cell survival with time and drug concentration. IC₅₀ values were estimated for each time point: we obtained 0.0830 ± 0.0043 , 0.0268 ± 0.0013 and 0.00204 ± 0.0005 µM at 24, 2° and 72 hours, respectively. The cytotoxicity of free DTXL was also tested on U87-1.4G cell monolayers cultured in a conventional 96 well-plates system. In this case, the cell viability was assessed via a standard MTT assay (Supplementary Figure 1). When the drig solution was changed daily, the measured IC_{50} values were 1.1822 ± 0.0025 at 48 hours and $0.1083 \pm 0.0008 \mu$ M at 72 hours. 24 hours after the DTXL supplementation, cell viability was close to 100% for all tested concentrations. Prolongation of the treatment resulted in cell viability of about 50% or higher. A similar trend was observed at all time points when the DTXL solution was not changed during the experiment. These results show that DTYL Las a higher cytotoxic effect on 3D organized cells, in the singlechannel microfluidic device, as compared to 2D cell monolayers, (50-fold lower IC₅₀ values). This trend of high chemosensitivity exhibited in 3D models was previously described in a study using bevacizumab when added to standard chemoradiation in phase III clinical trials exhibited marked radiosensitizing activity in the developed 3D model of GBM but no effect on 2D cells.[55] Moreover, a study investigating different cell lines from patients with head and neck squamous cell carcinoma revealed that LK0902 cells were more sensitive to cetuximab treatment in 3D conditions than cells grown in 2D.[56] Finally, this finding is also corroborated by Brito et

al.[53] where they observed that the efficiency of the treatment with Fmoc-Glc6P was higher in spheroids as compared to the conventional 2D cultures due to higher expression of glucose transporter 1 (GLUT1) by the cancer cells.

Figure 3.

3.2. Assessing the cytotoxicity of therapeutic agents in a double-shannel microfluidic device In the double-channel, the therapeutic solutions were added in the top channel (vascular compartment). The solutions reached the 3D tumor-like stated in the top compartment – cancer tissue compartment) by diffusion through the array of micropillar separating both channels (**Figure 1B**). The series of micropillars resembles ne vascular/tissue interface that confines the Matrigel matrix on the extravascular compartment while supporting the extravasation of nutrients, molecules, and nanoparticles. It is noteworthy to mention that the compartments in the present microfluidic device lay horizo. traffy on the same focal plane thus facilitating the image analysis.[31, 33] The biological barriers in the majority of microfluidic devices are realized by placing pre-fabricated porcus membranes in between two adjacent channels or compartments to reproduce a Boyden challer. Consequently, the two compartments lay on different focal planes and cannot be imaged simultaneously under a microscope.

Based on the data obtained for single-channel device, the cytotoxic effect of DTXL was examined only at the higher concentrations of 0.01, 0.1 and 10 μ M. In this double-channel configuration, we have also tested, DXTL-SPN (10 μ M of equivalent DTXL), and Fmoc-Glc6P (500 μ M). The viability of the U87-MG GFP+ cells was assessed at 24, 48 and 72 hours, following the variation in green fluorescence intensity as described above.

We did not observe cytotoxic effect of DXTL at concentration of 0.01 μ M for all tested time points (**Figure 4A**). At 0.1 μ M DXTL caused a significant decrease in cell viability after 72 hours (**Figure 4B and 4D**). At the highest tested concentration of 10 μ M, free DXTL induced an expressive decrease in cell viability in a time dependent manner (**Figures 4C and 4D**). In the double-channel microfluidic device, the cell viability is generally higher than 50% for the tested drug concentrations, except for 10 μ M DTXL at 72 hours. As such, IC₅₀ values cannot be estimated within the considered range. Reconstructed 3D images of the U87-MG GFP+ cells treated with 10 μ M free DXTL are presented in **Figure 4T** and demonstrate a progressive reduction in fluorescence intensity with prolongation of the treatment. Of note, the cytotoxic effect of DTXL at this concentration is significantly real ed in the double-channel microfluidic device as compared to the single-channel configuration. This difference could be ascribed to the lower concentration of DTXL reaching the tumor compartment in the double-channel chip because part of the infused drug is washed away via the vascular compartment.

Figure 4.

For assessing the cytotox sity of DTXL-SPN, only the highest DTXL dose was considered (10 μ M). The confocal microscopy images in **Figure 5A** show a decreasing cell survival over time. At all time points, the cell viability for the DTXL-SPN (**Figure 5B**) is comparable to that quantified with free DTXL (**Figure 4D**). Specifically, at 24 hours, the cell viability is 69 ± 30% for DTXL-SPN vs 80 ± 7% for free DTXL. This reduces to 64 ± 12% vs 57 ± 1% at 48 hours and to 56 ± 17% vs 40 ± 1% at 72 hours for DTXL-SPN and free DTXL, respectively. Using SPN stained with the red fluorescent dye Rhodamine-B (RhB-SPN), it was demonstrated that the

infused nanoparticles were able to permeate across the micropillar membrane and diffuse throughout the tumor-like matrix (**Figure 5**).

Figure 5.

Finally, the double-channel chip was also used to assess the therapeutic efficacy of a novel molecular compound – Fmoc-Glc6P for this type of cancer cells. The efficacy of this compound was originally demonstrated on osteosarcoma (SaOs-2) and breast cancer (MDA-MB-468) cell lines [52]. It acts as an efficient cancer antimetabolite by concomitant blocking the glucose transporter 1 (GLUT1) via specific interactions and form, ion of a nanonet serving as a physical barrier between the cancer cells and their environment [52-54]. The treatment is more efficient in spheroids as compared with 2D due o he higher GLUT1 expression in 3D cultures (Supplementary Figure 5) [51-54]. On note, GLUT1 is significantly upregulated both in vitro and in vivo GBM and thus, we hypothesized that this therapeutic will be also efficient in GBM [57, 58]. Indeed, Fmoc-Glc6P Comonstrated a strong anti-proliferative and cytotoxic effect on U87-MG cells cultured in 20 as well as in double-channel microfluidic chips. We selected a concentration of 500 µN for our experiments based on the previous studies with Fmoc-Glc6P [51]. As for the other therapeutic agents, Fmoc-Glc6P was infused into the vascular compartment. A significant drop in cell survival was observed over time (Figure 6A). After 72 hours only a few sparsely U87-MG GFP+ cells were visible in the channel. The quantitative results presented in Figure 6B show cell viability of $47 \pm 29\%$, $36 \pm 9\%$, and $19 \pm 13\%$, at 24, 48 and 72 hours, respectively. Similar trend was observed for 2D monolayers (Supplementary Figure 2). Furthermore, the effect of Fmoc-Glc6P compound on healthy brain cells – human

astrocytes – was assessed within the same double-channel microfluidic device (**Figures 6C**). The astrocytes were stained with the red fluorescein molecule Dil and their viability was assessed. We did not observe any toxic effect of Fmoc-Glc6P on human astrocytes (**Figures 6C and Figure 6D**) over time. This result indicates the high selectivity of Fmoc-Glc6P towards cancer cells.

Figure 6.

Free DTXL showed greater toxicity for U87-MG cells cut ared into single-channel microfluidic devices compared to those cultured in conventional 2D to onolayers. This confirms the potential of free DTXL to be injected *in situ* at the tumor s. C. Additionally, free DXTL and DTXL-SPNs are not efficient as Fmoc-Glc6P to induce U87-MG cell cytotoxicity when cultured into double-channel microfluidic device. Moreover, Fmoc-Glc6P targets specifically U87-MG cells without any deleterious effect in human astrocates. These findings demonstrate that double-channel can replicate better the vascular transport of systemically administered therapeutic agents and recreates closer the *in virtua* environment than 2D or single-channel configuration. Also, Fmoc-Glc6P demonstrates great potential to be applied systemically because acts specifically against cancer cells without causing adverse effects on healthy cells, combining a greater therapeutic efficacy with minor side effects.

4. Conclusions

Several chemotherapeutics, namely free DTXL, DTXL-SPN and Fmoc-Glc6P, were investigated using microfluidic chips. To elucidate the behavior and assess their anti-cancer

therapeutic efficacy in a more realistic scenario, we used single- and double-channel microfluidic devices simulating *in situ* and systemic administration, respectively. Importantly, the U87-MG cells cultured in 2D conditions are clearly more resistant to DTXL treatment, presenting IC_{50} 50-fold greater, as compared to those cultured into single-channel microfluidic chips. This study also clearly demonstrates the outstanding behavior of Fmoc-Glc6P, showing a selective effect on cells: inducing the death of GBM cancer cells, without eliciting deleterious effect on healthy/normal cells. Also, the effect of Fmoc-Glc6P, specifically on cancer cells cultured into double-channel microfluidic chips, show the potential of this model to articipate more closely the *in vivo* outcomes.

Overall, this study demonstrates the importance of mc ofluidic devices as a great predictive tool for modeling the *in situ* and systemic adminⁱs. ation of chemotherapy in GBM tumor and for developing new effective anti-cancer therapies.

AUTHOR INFORMATION

Corresponding author

*Email: ana.martins@iit.it

CRediT authorship contribution statement

A.M.M. is the main and the corresponding author of the manuscript and was involved in conception and design of all studies, from the execution and discussion of all experiments to the preparation, writing and correction of the manuscript. A.B. synthetized Fmoc-Glc6P and

performed the quantification of GLUT1 expression. M.G.B fabricated the microfluidic chips. A.F. produced and characterized the SPN. R.L.R. supported the experiments at the I3B's. I.P. and R.A.P. discussed the experiments, provided data on Fmoc-Glc6P, and corrected the manuscript. P.D. supported the experiments at IIT, discussed the experiments and wrote the manuscript. All the authors discussed the data.

Acknowledgements

This project was partially supported by the European Union's Horizon 2020 Research and Innovation Programme under the Marie Sklodowska-Corie grant agreement no. 754490 – MINDED. The authors thank the laboratory of Dr. Davide De Pietri Tonelli at the Fondazione Istituto Italiano di Tecnologia for providing U87-MG GFP+ cells; acknowledge Dr. Rui C. Pereira for his support on cell culture i. to .nicrofluidic chips and confocal microscopy; Dr. Michele Onetto and Dr. Marco Scotto for their assistance on confocal microscopy; and Dr. Martina Di Francesco for helping with by drawings of the microfluidic chips.

References

[1] G.M. Whitesides, The origins and the future of microfluidics, Nature 442(7101) (2006) 368-73.

[2] E.K. Sackmann, A.L. Fulton, D.J. Beebe, The present and future role of microfluidics in biomedical research, Nature 507(7491) (2014) 181-9.

[3] G. Vlachogiannis, S. Hedayat, A. Vatsiou, Y. Jamin, J. Fernandez-Mateos, K. Khan, A. Lampis, K. Eason, I. Huntingford, R. Burke, M. Rata, D.M. Koh, N. Tunariu, D. Collins, S. Hulkki-Wilson, C. Ragulan, I. Spiteri, S.Y. Moorcraft, I. Chau, S. Rao, D. Watkins, N. Fotiadis, M. Bali, M. Darvish-Damavandi, H. Lote, Z. Eltahir, E.C. Smyth, R. Begum, P.A. Clarke, J.C.

18

Hahne, M. Dowsett, J. de Bono, P. Workman, A. Sadanandam, M. Fassan, O.J. Sansom, S. Eccles, N. Starling, C. Braconi, A. Sottoriva, S.P. Robinson, D. Cunningham, N. Valeri, Patient-derived organoids model treatment response of metastatic gastrointestinal cancers, Science 359(6378) (2018) 920-926.

[4] A. Ranga, N. Gjorevski, M.P. Lutolf, Drug discovery through stem cell-based organoid models, Adv Drug Deliv Rev 69-70 (2014) 19-28.

[5] Y.S. Zhang, M. Duchamp, R. Oklu, L.W. Ellisen, R. Longer, A. Khademhosseini,
 Bioprinting the Cancer Microenvironment, ACS Biomater Sci Eng 2(10) (2016) 1710-1721.

[6] S.N. Bhatia, D.E. Ingber, Microfluidic organs-on-chips, Nat Biotechnol 32(8) (2014) 760-72.

[7] A.D. van der Meer, A. van den Berg, Organs-on-chip . breaking the in vitro impasse, Integr
Biol (Camb) 4(5) (2012) 461-70.

[8] T.E. Park, N. Mustafaoglu, A. Herland, R. Hasselkus, R. Mannix, E.A. FitzGerald, R. Prantil-Baun, A. Watters, O. Henry, M. Benz, H. Sanchez, H.J. McCrea, L.C. Goumnerova, H.W. Song, S.P. Palecek, E. Shusta, D.E. Ingber I ypoxia-enhanced Blood-Brain Barrier Chip recapitulates human barrier function and shurling of drugs and antibodies, Nat Commun 10 (2019).

[9] A. Herland, B.M. Macz, D. Das, M.R. Somayaji, R. Prantil-Baun, R. Novak, M. Cronce, T. Huffstater, S.S.F. Jean, M. Ingram, A. Chalkiadaki, D. Benson Chou, S. Marquez, A. Delahanty, S. Jalili-Firoozinezhad, Y. Milton, A. Sontheimer-Phelps, B. Swenor, O. Levy, K.K. Parker, A. Przekwas, D.E. Ingber, Quantitative prediction of human pharmacokinetic responses to drugs via fluidically coupled vascularized organ chips, Nat Biomed Eng 4(4) (2020) 421-436.

[10] C. Moraes, G. Mehta, S.C. Lesher-Perez, S. Takayama, Organs-on-a-chip: a focus on compartmentalized microdevices, Ann Biomed Eng 40(6) (2012) 1211-27.

[11] D. Huh, G.A. Hamilton, D.E. Ingber, From 3D cell culture to organs-on-chips, Trends Cell Biol 21(12) (2011) 745-54.

[12] A. Sontheimer-Phelps, B.A. Hassell, D.E. Ingber, Modelling cancer in microfluidic human organs-on-chips, Nat Rev Cancer 19(2) (2019) 65-81.

[13] S. Bersini, J.S. Jeon, G. Dubini, C. Arrigoni, S. Chung, J.L. Charest, M. Moretti, R.D.Kamm, A microfluidic 3D in vitro model for specificity of breast cancer metastasis to bone,Biomaterials 35(8) (2014) 2454-2461.

[14] M.R. Carvalho, D. Barata, L.M. Teixeira, S. Giselbrecht, K.L. Reis, J.M. Oliveira, R. Truckenmuller, P. Habibovic, Colorectal tumor-on-a-chip system: A 3D tool for precision onconanomedicine, Sci Adv 5(5) (2019).

[15] D. Caballero, S. Kaushik, V.M. Correlo, J M O iveira, R.L. Reis, S.C. Kundu, Organ-onchip models of cancer metastasis for fut re personalized medicine: From chip to the patient, Biomaterials 149 (2017) 98-115.

[16] H. Parsa, B.Z. Wang, G. Vun, a.-Novakovic, A microfluidic platform for the high-throughput study of pathological cardiac hypertrophy, Lab Chip 17(19) (2017) 3264-3271.

[17] S.S. Nunes, J.W. Miklos, L.Liu, R. Aschar-Sobbi, Y. Xiao, B. Zhang, J. Jiang, S. Masse, M. Gagliardi, A. Hsieh, N. Pavandiran, M.A. Laflamme, K. Nanthakumar, G.J. Gross, P.H. Backx, G. Keller, M. Radisic, Biowire: a platform for maturation of human pluripotent stem cell-derived cardiomyocytes, Nat Methods 10(8) (2013) 781-7.

[18] J.-S. Chen, P.-F. Chen, H.T.-H. Lin, N.-T. Huang, A Localized surface plasmon resonance (LSPR) sensor integrated automated microfluidic system for multiplex inflammatory biomarker detection, Analyst 145(23) (2020) 7654-7661.

[19] M.G. Barbato, R.C. Pereira, H. Mollica, A. Palange, M. Ferreira, P. Decuzzi, A permeable on-chip microvasculature for assessing the transport of macromolecules and polymeric nanoconstructs, Journal of Colloid and Interface Science 594 (2021) 409-423.

[20] B. Buchroithner, S. Mayr, F. Hauser, E. Priglinger, H. Stangl, A.R. Santa-Maria, M.A. Deli,A. Der, T.A. Klar, M. Axmann, Dual Channel Microfluidics for Mimicking the Blood–BrainBarrier, ACS nano 15(2) (2021) 2984-2993.

[21] F. Yu, D. Nivasini, O.S. Kumar, D. Choudhury, L.C. Foo, S.A. Ng, Microfluidic platforms for modeling biological barriers in the circulatory system, Drug Liscovery today 23(4) (2018) 815-829.

[22] S.N. Bhatia, D.E. Ingber, Microfluidic organs-on-ci os, Nat Biotechnol 32(8) (2014) 760-772.

[23] K.H. Benam, R. Villenave, C. Lucchesi A. Varone, C. Hubeau, H.H. Lee, S.E. Alves, M. Salmon, T.C. Ferrante, J.C. Weaver, A. Pahinski, G.A. Hamilton, D.E. Ingber, Small airway-ona-chip enables analysis of human lung inflammation and drug responses in vitro, Nature Methods 13(2) (2016) 151-+.

[24] M.B. Chen, J.A. Whisher, J. Frose, C. Yu, Y. Shin, R.D. Kamm, On-chip human microvasculature assay ter visualization and quantification of tumor cell extravasation dynamics, Nat Protoc 12(5) (2017) 865-880.

[25] K. Funamoto, I.K. Zervantonakis, Y. Liu, C.J. Ochs, C. Kim, R.D. Kamm, A novel microfluidic platform for high-resolution imaging of a three-dimensional cell culture under a controlled hypoxic environment, Lab Chip 12(22) (2012) 4855-63.

[26] T. Osaki, V. Sivathanu, R.D. Kamm, Engineered 3D vascular and neuronal networks in a microfluidic platform, Sci Rep 8(1) (2018) 5168.

[27] B. Zhang, B.F.L. Lai, R. Xie, L. Davenport Huyer, M. Montgomery, M. Radisic, Microfabrication of AngioChip, a biodegradable polymer scaffold with microfluidic vasculature, Nat Protoc 13(8) (2018) 1793-1813.

[28] Y. Choi, E. Hyun, J. Seo, C. Blundell, H.C. Kim, E. Lee, S.H. Lee, A. Moon, W.K. Moon,D. Huh, A microengineered pathophysiological model of early-stage breast cancer, Lab Chip 15(16) (2015) 3350-7.

[29] I.K. Zervantonakis, S.K. Hughes-Alford, J.L. Charest, J.S. Condeelis, F.B. Gertler, R.D. Kamm, Three-dimensional microfluidic model for tumor conclustravasation and endothelial barrier function, Proc Natl Acad Sci U S A 109(34) (2012) 13515-20.

[30] A. Pavesi, A.T. Tan, M.B. Chen, G. Adriani, A. Ber, 'etti, R.D. Kamm, Using microfluidics to investigate tumor cell extravasation and T-cell 'm'aunotherapies, Conf Proc IEEE Eng Med Biol Soc 2015 (2015) 1853-6.

[31] H. Mollica, R. Palomba, R. Prin avera, P. Decuzzi, Two-Channel Compartmentalized Microfluidic Chip for Real-Time Munitoring of the Metastatic Cascade, Acs Biomaterials Science & Engineering 5(9) (20.9) 4334-4843.

[32] S.A. Roberts, A.E. Walin, N. Agrawal, Development of a Single-Cell Migration and Extravasation Platform unrough Selective Surface Modification, Anal Chem 88(5) (2016) 2770-6.

[33] C. Manneschi, R.C. Pereira, G. Marinaro, A. Bosca, M. Francardi, P. Decuzzi, A microfluidic platform with permeable walls for the analysis of vascular and extravascular mass transport, Microfluid Nanofluid 20(8) (2016).

[34] H. Mollica, A. Coclite, M.E. Miali, R.C. Pereira, L. Paleari, C. Manneschi, A. DeCensi, P. Decuzzi, Deciphering the relative contribution of vascular inflammation and blood rheology in metastatic spreading, Biomicrofluidics 12(4) (2018).

[35] M. Colasuonno, A.L. Palange, R. Aid, M. Ferreira, H. Mollica, R. Palomba, M. Emdin, M. Del Sette, C. Chauvierre, D. Letourneur, P. Decuzzi, Erythrocyte-Inspired Discoidal Polymeric Nanoconstructs Carrying Tissue Plasminogen Activator for the Enhanced Lysis of Blood Clots, ACS Nano 12(12) (2018) 12224-12237.

[36] V. Lusi, T.L. Moore, F. Laurino, A. Coclite, R. Perreira, M. Ferreira, I. Rizzuti, R. Palomba,
P. Zunino, M. Duocastella, S. Mizrahy, D. Peer, P. Decuzz, A tissue chamber chip for assessing nanoparticle mobility in the extravascular space, Biomed Cacrodevices 21(2) (2019).

[37] D. Di Mascolo, S. Varesano, R. Benelli, H 1 ^{*}ol¹.ca, A. Salis, M.R. Zocchi, P. Decuzzi, A. Poggi, Nanoformulated Zoledronic Acid Loo' is the Vδ2 T Cell Immunotherapeutic Potential in Colorectal Cancer, Cancers 12(1) (2020) ¹04.

[38] U.Y. Schaff, M.M. Xing, K.K Lin N. Pan, N.L. Jeon, S.I. Simon, Vascular mimetics based on microfluidics for imaging the leukocyte--endothelial inflammatory response, Lab Chip 7(4) (2007) 448-56.

[39] T. Omori, Y. Ima, K. Kikuchi, T. Ishikawa, T. Yamaguchi, Hemodynamics in the microcirculation and in microfluidics, Ann Biomed Eng 43(1) (2015) 238-57.

[40] H. Mollica, A. Coclite, M.E. Miali, R.C. Pereira, L. Paleari, C. Manneschi, A. DeCensi, P. Decuzzi, Deciphering the relative contribution of vascular inflammation and blood rheology in metastatic spreading, Biomicrofluidics 12(4) (2018) 042205.

[41] O.C. Farokhzad, A. Khademhosseini, S. Jon, A. Hermmann, J. Cheng, C. Chin, A. Kiselyuk, B. Teply, G. Eng, R. Langer, Microfluidic system for studying the interaction of nanoparticles and microparticles with cells, Anal Chem 77(17) (2005) 5453-9.

[42] G.D. Vatine, R. Barrile, M.J. Workman, S. Sances, B.K. Barriga, M. Rahnama, S. Barthakur, M. Kasendra, C. Lucchesi, J. Kerns, N. Wen, W.R. Spivia, Z. Chen, J. Van Eyk, C.N. Svendsen, Human iPSC-Derived Blood-Brain Barrier Chips Enable Disease Modeling and Personalized Medicine Applications, Cell Stem Cell 24(6) (2019) 5>5-1005 e6.

[43] T.F. Cloughesy, W.K. Cavenee, P.S. Mischel, Glioblastoma. From Molecular Pathology to Targeted Treatment, Annu Rev Pathol-Mech 9 (2014) 1-25.

[44] H.L. Gao, J. Qian, Z. Yang, Z.Q. Pang, Z.J. Xi, S.J. Cao, Y.C. Wang, S.Q. Pan, S. Zhang,
W. Wang, X.G. Jiang, Q.Z. Zhang, Vino e-cell SELEX aptamer-functionalised poly(ethyleneglycol)-poly(epsilon-caprola tors) nanoparticles for enhanced targeted glioblastoma therapy, Biomaterials 33(20) (2012) 6264-6272.

[45] H.L. Gao, S. Zhang, Z. Yang, C. Cao, X.G. Jiang, Z.Q. Pang, In vitro and in vivo intracellular distribution and onti-glioblastoma effects of docetaxel-loaded nanoparticles functioned with IL-13 peptide, Lt J Pharmaceut 466(1-2) (2014) 8-17.

[46] C. Stigliano, J. Yey, M. Ramirez, S. Aryal, P. Decuzzi, Radiolabeled Polymeric Nanoconstructs Loaded with Docetaxel and Curcumin for Cancer Combinatorial Therapy and Nuclear Imaging, Adv Funct Mater 25(22) (2015) 3371-3379.

[47] A. Lee, D. Di Mascolo, M. Francardi, F. Piccardi, T. Bandiera, P. Decuzzi, Spherical polymeric nanoconstructs for combined chemotherapeutic and anti-inflammatory therapies, Nanomed-Nanotechnol 12(7) (2016) 2139-2147.

[48] D. Di Mascolo, A.L. Palange, R. Primavera, F. Macchi, T. Catelani, F. Piccardi, R. Spanò,

M. Ferreira, R. Marotta, A. Armirotti, Conformable hierarchically engineered polymeric micromeshes enabling combinatorial therapies in brain tumours, Nature Nanotechnology 16(7) (2021) 820-829.

[49] K. Gelmon, The Taxoids - Paclitaxel and Docetaxel, Lancet 344(8932) (1994) 1267-1272.

[50] I.E. Kuppens, Current state of the art of new tubulin inhibitors in the clinic, Curr Clin Pharmacol 1(1) (2006) 57-70.

[51] R.A. Pires, Y.M. Abul-Haija, D.S. Costa, R. Novoa-Carballal, R.L. Reis, R.V. Ulijn, I. Pashkuleva, Controlling Cancer Cell Fate Using Localized Biocatalytic Self-Assembly of an Aromatic Carbohydrate Amphiphile, J Am Chem Soc 137(2) (2015) 576-579.

[52] A. Brito, P.M.R. Pereira, D. Soares da Cos⁺a, K.J. Reis, R.V. Ulijn, J.S. Lewis, R.A. Pires, I. Pashkuleva, Inhibiting cancer metaboli m by aromatic carbohydrate amphiphiles that act as antagonists of the glucose transporter GLUT1 Chemical Science (2020).

[53] A. Brito, P. Pereira, R. Reis, R. Ulijn, J.S. Lewis, R.A. Pires, I. Pashkuleva, Aromatic carbohydrate amphiphile disrupt: cancer spheroids and prevents relapse, Nanoscale (2020).

[54] A. Brito, S. Kasser, K.L. Reis, R.V. Ulijn, R.A. Pires, I. Pashkuleva, Carbohydrate amphiphiles for supramelecular biomaterials: Design, self-assembly, and applications, Chem 7(11) (2021) 2943-2964.

[55] N. Gomez-Roman, K. Stevenson, L. Gilmour, G. Hamilton, A.J. Chalmers, A novel 3D human glioblastoma cell culture system for modeling drug and radiation responses, Neurooncology 19(2) (2017) 229-241.

[56] S. Melissaridou, E. Wiechec, M. Magan, M.V. Jain, M.K. Chung, L. Farnebo, K. Roberg, The effect of 2D and 3D cell cultures on treatment response, EMT profile and stem cell features in head and neck cancer, Cancer cell international 19(1) (2019) 16.

[57] T. Nishioka, Y. Oda, Y. Seino, T. Yamamoto, N. Inagaki, H. Yano, H. Imura, R. Shigemoto, H. Kikuchi, Distribution of the glucose transporters in human brain tumors, Cancer research 52(14) (1992) 3972-3979.

[58] F. Pistollato, S. Abbadi, E. Rampazzo, L. Persano, A. Della Fuppa, C. Frasson, E. Sarto, R. Scienza, D. D'avella, G. Basso, Intratumoral hypoxic gradient drives stem cells distribution and MGMT expression in glioblastoma, Stem cells 28(5) (2010, 851-862.

[59] M. Akay, J. Hite, N.G. Avci, Y. Fan, Y. Akay, G L , J.J. Zhu, Drug Screening of Human GBM Spheroids in Brain Cancer Chip, Sci Rep ⁹(1) (2018) 15423.

[60] S. Bang, S. Lee, N. Choi, H.N. Kim, Imraging Brain- Pathophysiology- Mimetic Platforms for Studying Neurodegenerative Disease.¹ Brain Organoids and Brains- on- a- Chip, Advanced Healthcare Materials 10(12) (2021) 20(2119.

[61] Z. Hu, Y. Cao, E.A. Gala., L. Hao, H. Zhao, J. Tang, G. Sang, H. Wang, B. Xu, S. Ma, Vascularized Tumor Spheroid-on-a-Chip Model Verifies Synergistic Vasoprotective and Chemotherapeutic Effect. ACS Biomaterials Science & Engineering 8(3) (2022) 1215-1225.

Figure Captions

Figure 1. Single- and double-channel microfluidic devices. A. Schematic representation of the single-channel device, including a scanning electron microscopy (SEM) micrograph of the channel and a confocal image of U87-MG GFP+ cells cultured in Matrigel matrix. **B**. Schematic representation of a double-channel device, including a SEM micrograph of the two-channels (extravascular and vascular compartments). The bottom-right inset gives a SEM image of the micropillars realizing the permeable membrane between the two-compartments. (Scale bar: 100 μ m, except for the micropillar image - bottom right - 10 μ m).

Figure 2. Therapeutic agents. A. Chemical structure of docetaxel (DTXL). **B**. Schematic representation of the spherical polymeric nanoparacies (SPN) loaded with docetaxel (DTXL-SPN); diameter and Z-Potential, size distabut on measured by Dynamic Light scattering (DLS), the release profile at 37 °C in physiological solution (PBS, pH 7.4); and (C) 500 μM Fmoc-Glc6P for 24, 48 and 72 hours **C** Chemical structure of the aromatic N-glucoside N-(fluorenylmethoxycarbonyl)-glucosanine-6-phosphate (Fmoc-Glc6P).

Figure 3. Human brain umor cell viability analysis in single-channel microfluidic devicefree DTXL. A-E. Representative confocal fluorescent microscopy images of U87-MG GFP+ cells cultured in Matrigel and exposed to different doses of free DTXL (0.01, 0.05, 0.1, 1 and 10 μ M) at different time points (24, 48 and 72 hours). The scale bar is 50 μ m and applies to all images. F. Cell viability analyses and IC₅₀ values determined for the different time points. Results are expressed as mean \pm SD (n = 5 per time point). All concentrations presented a significant difference over time compared to control (no treatment) except at 0.01 μ M after 24 and 48h hours. *: p < 0.01 and ** p < 0.05 between different concentrations in the same time point; ##: p < 0.05 for the same concentration of DTXL at different time points).

Figure 4. Human brain tumor cell viability analysis in double-channel microfluidic device – free DTXL. A-C. Representative confocal fluorescent microscopy images of U87-MG cells cultured in Matrigel and exposed to different doses of free DTXL (0.1, 1 and 10 μ M) at different time points (24, 48 and 72 hours). D. Cell viability analyses determined for the different time points. Results are expressed as mean \pm SD (n = 4 per time point) E. 3D-Reconstruction of confocal fluorescent images showing the U87-MG GFF. cells at different time points post exposure to 10 μ M DTXL. (Scale bar: 100 μ m. *: p < 0 of over time).

Figure 5. Human brain tumor cell vial lity analysis in double-channel microfluidic device – DTXL-SPN. A. Representative contocal fluorescent microscopy images of U87-MG GFP+ cells cultured in Matrigel and exposed to SPN loaded with 10 μ M DTXL (DTXL-SPN), at different time points (24, 48 and 72 hours). B. Cell viability analyses determined for the different culturing conditions. Respire and expressed as mean \pm SD (n = 4 per time point). *: p < 0.01 compared with the control (no treatment). C. Representative confocal fluorescent microscopy images at 72 hours showing U87-MG GFP+ (green dots) and RhB-SPN (red dots) next to the micropillars. (Scale bar: 100 μ m).

Figure 6. Human brain tumor cell and astrocytes viability analysis in double-channel microfluidic device – **Fmoc-Glc6P. A.** Representative confocal fluorescent microscopy images of U87-MG GFP+ cells cultured in Matrigel and exposed to 500 μM of Fmoc-Glc6P, at different

time points (24, 48 and 72 hours). **B.** Representative confocal fluorescent microscopy images of astrocytes stained with Dil, cultured in Matrigel and exposed to 500 μ M of Fmoc-Glc6P, at different time points (24, 48 and 72 hours). **C,D.** Cell viability analyses determined for the different culturing conditions of the U87-MG cells GFP+ and human astrocytes stained with Dil. Results are expressed as mean \pm SD (n = 4 per time point). *: p < 0.01 compared with the control (only EMEM). (Scale bar: 100 μ M).

Declaration of interests

.

The authors declare that they have no known competing financial interests or personal relationships that could have appeared to influence the work reported in this paper.

⊠The authors declare the following financial interests/personal relationships which may be considered as potential competing interests:

Ana Martins reports financial support was provided by European Commission. Ana Martins reports a relationship with European Commission that includes: funding grants.

Solution of the second second